





## Article

# Numerical Study of Natural Convection of Biological Nanofluid Flow Prepared from Tea Leaves under the Effect of Magnetic Field

Yacine Khetib <sup>1,2</sup>, Ahmad Alahmadi <sup>3</sup>, Ali Alzaed <sup>4</sup>, Hussein A. Saleem <sup>5</sup>, Mohsen Sharifpur <sup>6,7,\*</sup>  
and Goshtasp Cheraghian <sup>8,\*</sup>

- <sup>1</sup> Mechanical Engineering Department, Faculty of Engineering, King Abdulaziz University, Jeddah 80204, Saudi Arabia; ykhetib@yahoo.com  
<sup>2</sup> Center Excellence of Renewable Energy and Power, King Abdulaziz University, Jeddah 80204, Saudi Arabia  
<sup>3</sup> Department of Electrical Engineering, College of Engineering, Taif University, Taif 21944, Saudi Arabia; aziz@tu.edu.sa  
<sup>4</sup> Architectural Engineering Department, Faculty of Engineering, Taif University, Taif 21944, Saudi Arabia; alzaed@tu.edu.sa  
<sup>5</sup> Mining Engineering Department, Faculty of Engineering, King Abdulaziz University, Jeddah 80204, Saudi Arabia; hselem2002@yahoo.com  
<sup>6</sup> Department of Mechanical and Aeronautical Engineering, University of Pretoria, Pretoria 0002, South Africa  
<sup>7</sup> Department of Medical Research, China Medical University Hospital, China Medical University, Taichung 404, Taiwan  
<sup>8</sup> Independent Researcher, 38106 Braunschweig, Germany  
\* Correspondence: mohsen.sharifpur@up.ac.za (M.S.); goshtasbc@gmail.com (G.C.)



**Citation:** Khetib, Y.; Alahmadi, A.; Alzaed, A.; Saleem, H.A.; Sharifpur, M.; Cheraghian, G. Numerical Study of Natural Convection of Biological Nanofluid Flow Prepared from Tea Leaves under the Effect of Magnetic Field. *Processes* **2021**, *9*, 1824. <https://doi.org/10.3390/pr9101824>

Academic Editor: Alfredo Iranzo

Received: 2 August 2021

Accepted: 28 August 2021

Published: 14 October 2021

**Publisher's Note:** MDPI stays neutral with regard to jurisdictional claims in published maps and institutional affiliations.



**Copyright:** © 2021 by the authors. Licensee MDPI, Basel, Switzerland. This article is an open access article distributed under the terms and conditions of the Creative Commons Attribution (CC BY) license (<https://creativecommons.org/licenses/by/4.0/>).

**Abstract:** The heat transfer of a biological nanofluid ( $N/F$ ) in a rectangular cavity with two hot triangular blades is examined in this work. The properties used for nanoparticles ( $N/Ps$ ) are derived from a  $N/P$  prepared naturally from tea leaves. Silver  $N/Ps$  are distributed in a 50–50 water/ethylene glycol solution. The cavity's bottom wall is extremely hot, while the upper wall is extremely cold. The side walls are insulated, and the enclosure is surrounded by a horizontal magnetic field ( $M/F$ ). The equations are solved using the control volume technique and the SIMPLE algorithm. Finally, the  $Nu$  is determined by changing the dimensions of the blade, the Rayleigh number ( $Ra$ ), and the Hartmann number ( $Ha$ ). Finally, a correlation is expressed for the  $Nu$  in the range of parameter changes. The results demonstrate that an increment in the  $Ra$  from  $10^3$  to  $10^5$  enhances the  $Nu$  more than 2.5 times in the absence of an  $M/F$ . An enhancement in the strength of the  $M/F$ , especially at the  $Ra$  of 105, leads to a dramatic reduction in the  $Nu$ . An increase in the height of the triangular blade intensifies the amount of  $Nu$  in weak and strong convection. The enlargement of the base of the triangular blade first enhances and then decreases as the  $Nu$ . The addition of 5% silver biological  $N/Ps$  to the fluid enhances the  $Nu$  by 13.7% in the absence of an  $M/F$  for high  $Ras$ .

**Keywords:** triangular blade; natural convection; magnetic field; biological nanofluid

## 1. Introduction

Free convection and forced convection are two different types of convective heat transfer ( $H/T$ ) which are used in many fields such as cooling [1–7], solar systems [8–11], and nanofluid-based systems [12–14]. In forced convection, an external machine such as a pump, fan, or compressor is employed to flow the fluid, but in free convection, one does not need an external force to move the fluid, and the fluid moves due to the density gradient. Since no external force is required to flow the fluid, this type of  $H/T$  is widely used in low-energy devices [15–19]. Some industrial appliances that do not use electricity employ this type of  $H/T$  to transfer heat, for cooling or heating. Cooking ovens, industrial ovens, cooling in industrial refrigerators, etc., are some applications of  $H/T$  in the industry

and in the daily life of human beings. Many researchers have used closed cavities to investigate this type of  $H/T$  [20–22]. Therefore, different researchers have studied cavities with different shapes [23–25]. The cavities with more complex shapes such as triangles, etc., have attracted less attention. Pordanjani and Aghakhani [26] showed that an enhancement in the Rayleigh number ( $Ra$ ) enhances the free convection and increases the rate of  $H/T$  in a complex closed cavity. In another study, Das et al. [1] evaluated the impact of the Rayleigh number on the flow field. In addition, Sheremet et al. [4] determined the amount of Nusselt number in an enclosure by changing the Rayleigh number. The influence of changes in fluid flow and the amount of stream function with the Rayleigh number has been studied by Aghakhani et al. [3]. The results of the article [4] demonstrated that an increment in the Rayleigh number improves free convective heat transfer.

The study of nanofluids ( $N/Fs$ ) is one of the areas that has gotten a lot of scientific interest in the recent two decades [27–30]. Water is mainly used for cooling various devices in small and large industries. Water is available and cheap. Its THCO, on the other hand, is poor, limiting its  $H/T$ . Enhancing the THCO of  $H/T$  by dispersing various nanoparticles ( $N/Ps$ ) in it is one approach to boost it. [31–33]. Ethylene glycol (EG) is also used as antifreeze in many industries but also has low THCO. Hence, different  $N/Ps$  are added to this fluid to intensify its THCO. So far, many researchers have used  $N/Fs$  in their research [34–39]. There are many articles on nanofluids. The effect of nanofluid on Nusselt number was investigated by Rahimi et al. [2]. In addition, in another article by Revnic et al. [6], the influence of the presence of nanofluid on heat transfer was investigated. Rahimi et al. [1] studied the average Nusselt number by changing the volume percentage of nanoparticles and revealed that adding nanoparticles to the base fluid can increase the amount of heat transfer. Among these, the type of  $N/Ps$  is also important. In recent years, the use of biological  $N/Ps$  has received more attention from researchers [40,41]. These  $N/Ps$  are eco-friendly and can be prepared from environmental materials. Therefore, some researchers have used this type of  $N/Fs$  in their research [42,43]. In one of these studies conducted by Bahiraie and Heshmatian [44], the effect of using eco-friendly silver/water  $N/F$  on the efficiency of a heat exchanger was investigated. The results of this study showed that the use of this biological  $N/F$  is effective in the improvement of  $H/T$ .

One of the most important factors influencing  $H/T$  is the magnetic field ( $M/F$ ) [45–47]. The  $M/F$  is generally present in various industries due to the presence of electricity. Therefore, it is necessary to study the effect of this external source on  $H/T$ . In some research, it enhances [48] or reduces [49] the  $H/T$  based on the geometry of the cavity. Therefore, various researchers have studied the effect of the  $M/F$  in different geometries of cavities [50–52]. The effect of the magnetic field on fluid flow was numerically studied by Afrand [15]. In another study, the impact of the magnetic field on the heat transfer rate was investigated by Selimefendigil and Öztop [20]. It was found that the heat transfer rate is reduced by applying the magnetic field. Selimefendigil and Öztop [21] also studied the influence of the Hartmann number on heat transfer and the Nusselt number. In one of these studies, Aminossadati [49] studied the  $H/T$  of copper/water  $N/F$  in a triangular cavity under an  $M/F$  using the SIMPLE algorithm numerically. In the middle of the cavity, there was a cavity-shaped heat source that heats the fluid inside the cavity. The results demonstrated that an increment in the  $Ra$ , a reduction in the Hartmann number ( $Ha$ ), and a decrease in the distance between the heat source and the cold wall improve the thermal efficiency.

Today, the use of  $N/Fs$  is much higher than before. Therefore, the environmental consideration of using  $N/Ps$  is one of the challenges in this field that can be considered. The use of biological  $N/Ps$  can prevent damage to the environment. On the other hand, due to the importance of natural convection in industry, this paper investigates the effect of using biological  $N/F$  of silver in 50–50 EG/water on natural convection under the effect of an  $M/F$  in a cavity with two triangular blades. In addition, to find the best case for maximum  $H/T$ , the effect of  $Ra$ ,  $Ha$ , blade height, and width on  $Nu$  is studied. The innovation of the present work is to find the highest rate of  $H/T$  by changing the geometry of the blade in a

cavity with a new geometry under the impact of the  $M/F$  in the presence of the biological  $N/F$ . Finally, a correlation is given for the  $Nu$ .

## 2. Problem Description

As shown in Figure 1, the cavity is a rectangle with a length-to-width ratio of 3. On the cavity bottom wall, two triangular blades with a  $W$ -height and an  $H$ -base are placed. There is an Ag/water-EG (50–50)  $N/F$  inside the enclosure. Silver  $N/Ps$  are biologically prepared from tea leaves. The preparation process of  $N/Ps$  is shown in Figure 2. The upper wall is at  $T_c$  and the lower one and the blades are at  $T_H$ . The side walls are also insulated. There is also a horizontal  $M/F$  next to the enclosure.

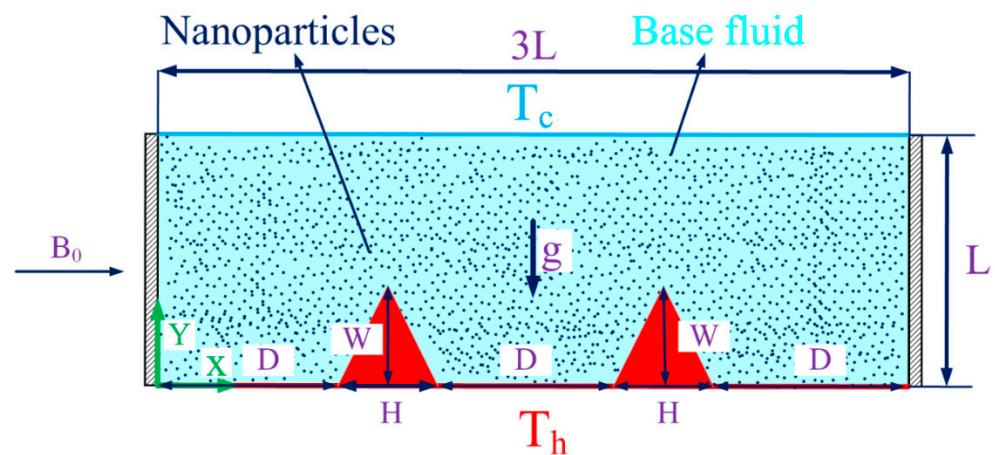


Figure 1. General schematic of the cavity.

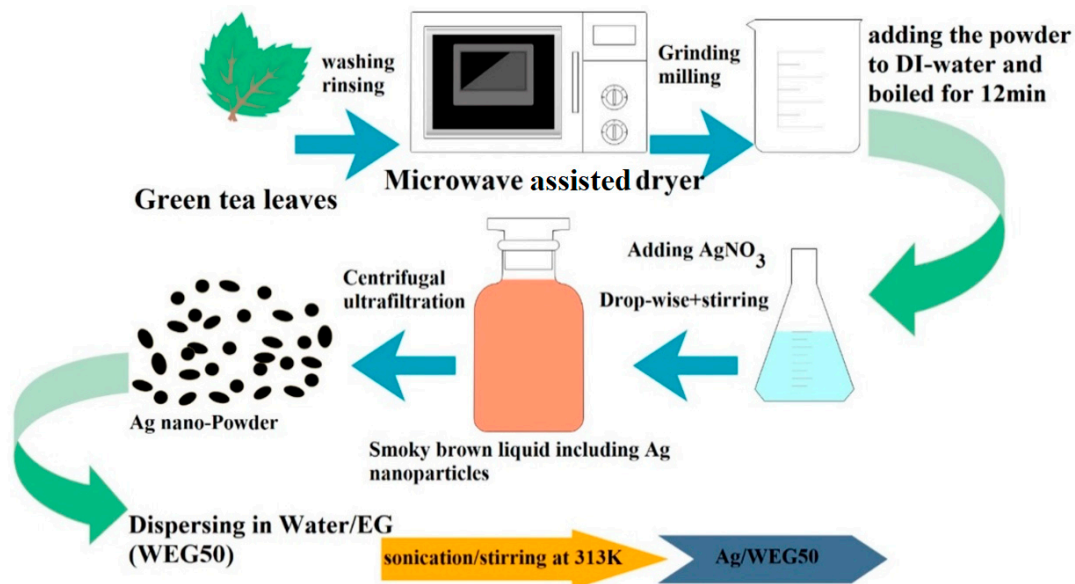


Figure 2. The preparation process of  $N/Ps$  from tea leaves.

### 2.1. Governing Equations and Boundary Conditions

To non-dimensionalize the equations, use the following dimensionless parameters:

$$X, Y = \frac{x, y}{l}, L, W, H = \frac{L, W, H}{l}, U = \frac{ul}{\alpha_f}, V = \frac{vl}{\alpha_f}, P = \frac{pl^2}{\rho_f \alpha_f^2}, \theta = \frac{T - T_c}{T_h - T_c} \quad (1)$$

$$Pr = \frac{\rho_f \alpha_f}{\mu_f}, Ra = \frac{g \beta_f l^3 (T_h - T_c) \rho_f}{\mu_f \alpha_f}, Ha^2 = \frac{\sigma_f B_0^2 l^2}{\mu_f}$$

The two-dimensional equations that govern the fluid flow are as follows. These equations are constructed using a laminar and steady flow and a Newtonian incompressible fluid as assumptions. It is worth noting that the buoyancy force is approximated using the Boussinesq approximation. The effect of viscosity loss and radiation  $H/T$  is neglected [53,54]:

$$U_X + V_Y = 0 \quad (2)$$

$$UU_X + VU_Y = -p_X + \frac{\mu_{nf}}{\rho_{nf}\alpha_f}(U_{XX} + U_{YY}) \quad (3)$$

$$UV_X + VV_Y = -p_Y + \frac{\mu_{nf}}{\rho_{nf}\alpha_f}(V_{XX} + V_{YY}) + \frac{\beta_{nf}}{\beta_f}RaPr\theta - \frac{\rho_f}{\rho_{nf}}\frac{\sigma_{nf}}{\sigma_f}PrHa^2V \quad (4)$$

$$U\theta_X + V\theta_Y = \frac{\alpha_{nf}}{\alpha_f}(\theta_{XX} + \theta_{YY}) \quad (5)$$

The dimensionless boundary conditions are shown in Figure 3.

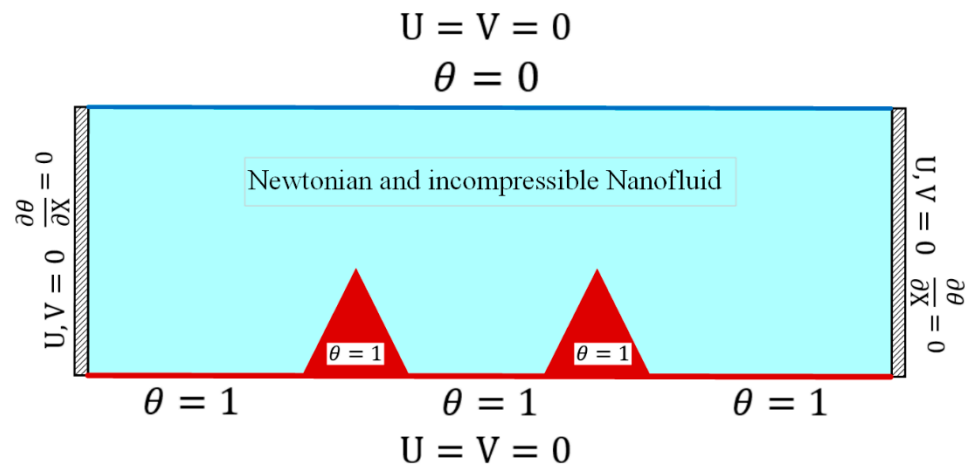


**Figure 3.** Dimensionless boundary conditions.

To obtain the amount of  $H/T$ , the  $Nu$  on top wall is calculated as follows:

$$Nu_x = \frac{h3L}{k_f} \quad (6)$$

$$h = \frac{q_w}{T_h - T_c} \quad (7)$$

$$q_w = k_{nf} \left( \frac{\partial T}{\partial X} \right) \quad (8)$$

The definition of a local  $Nu$  on top wall for a  $N/F$  is:

$$Nu_X = -\frac{k_{nf}}{k_f} \left( \frac{\partial \theta}{\partial X} \right) \quad (9)$$

The following equation is used to estimate the average  $Nu$  on a cold wall:

$$Nu = \frac{1}{3L} \int_0^{3L} Nu_X dY = -\frac{1}{3L} \frac{k_{nf}}{k_f} \int_0^{3L} \frac{\partial \theta}{\partial X} dY \quad (10)$$

## 2.2. $N/F$ Properties Equations

The relationships used to obtain  $N/F$  properties other than THCO are given as follows [55,56]:

$$\sigma_{nf} = (1 - \phi)\sigma_f + \phi\sigma_{Ag} \quad (11)$$

$$\rho_{nf} = (1 - \varphi)\rho_f + \varphi\rho_{Ag} \quad (12)$$

$$(\rho\beta)_{nf} = (1 - \varphi)(\rho\beta)_f + \varphi(\rho\beta)_{Ag} \quad (13)$$

$$(\rho c_p)_{nf} = (1 - \varphi)(\rho c_p)_f + \varphi(\rho c_p)_{Ag} \quad (14)$$

$$\alpha_{nf} = \frac{k_{nf}}{(\rho c_p)_{nf}} \quad (15)$$

$$\frac{\mu_{nf}}{\mu_f} = 1 + 2.5\varphi \quad (16)$$

Biological silver N/Ps obtained from tea leaves are used to prepare the N/F. The THCO of the biological N/F is [57]:

$$\frac{k_{nf}}{k_f} = 0.981 + 0.00114 \times T + 30.661 \times \varphi \quad (17)$$

The rest of the properties of EG and silver N/Ps are given in Table 1.

**Table 1.** Thermophysical properties of water-EG and A [43,56,58–60].

	$c_p$ (J/kg·K)	$k$ (W/m·K)	$\rho$ (kg/m <sup>3</sup> )	$\mu$ (kg/m·s)	$\sigma$ (Ω·m) <sup>−1</sup>	$d_{Ag}$ (nm)
Water	4179	0.613	997.1	0.001	0.05	-
EG	2430.8	0.2532	1088	0.0141	$9.2 \times 10^{-5}$	-
Ag	235	429	10,500	-	$1.6 \times 10^{-4}$	40

### 2.3. Numerical Procedure

To solve the equations, they are non-dimensionalized and then solved using dimensionless boundary conditions. The equations are discretized using the volume control approach first, and then solved in FORTRAN using the SIMPLE algorithm. The convergence criterion for all equations is assumed to be  $10^{-8}$ .

It is important to do a good grid analysis in order to answer the equations. A structured square mesh is utilized for this purpose. Various simulations are carried out in order to assess the solution's independence from the grid. For example, the average  $Nu$  is presented in Table 2 for different grids when  $Ra = 10^5$ ,  $Ha = 0$ , and  $W = H = 0.2$ . Due to the changes in the  $Nu$ , the grid resolution of  $150 \times 450$  is selected for the simulations.

**Table 2.** The average  $Nu$  for different computational grids when  $Ra = 10^5$ ,  $Ha = 0$ , and  $W = H = 0.2$ .

Element	$90 \times 270$	$110 \times 330$	$130 \times 390$	$150 \times 450$	$170 \times 510$
$Nu$	4.89	5.41	5.12	4.99	4.99

### 2.4. Validation

To confirm the correctness of the simulations, it is important to compare the results to those of other previously reported research. When the findings of this study are compared to those of other studies, valid conclusions are reached. For example, the results of Oztop and Abu-Nada [61], who examined free convection  $H/T$ , are compared. Figure 4 shows the average  $Nu$  findings for various volume fractions and  $Ras$ . The results are in good agreement and there is just a little difference between them, as can be seen in Figure 4.

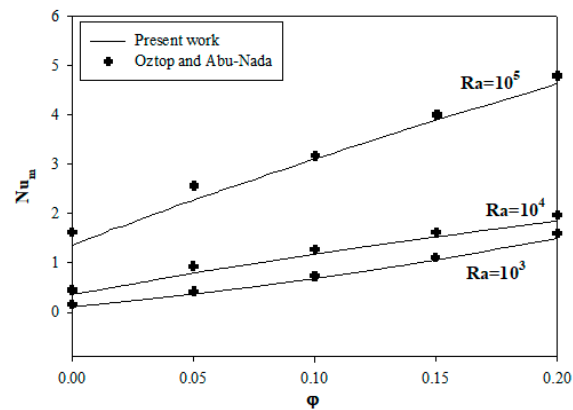


Figure 4. The average  $Nu$  for different volume fractions and various  $Ras$ .

### 3. Results and Discussion

Figure 5 shows the velocity contours for different  $Ra$  and  $Ha$ ,  $W = 0.8$ ,  $H = 0.2$ , and 3% biological  $N/Ps$ . The numerical values of the stream function are higher for higher  $Ras$ . In addition, higher numerical values of the stream function correspond to lower  $Has$ . The minimum value of the stream function is found at  $Ra = 10^3$  and  $Ha = 60$ , while the maximum stream function occurs at  $Ra = 10^6$  and  $Ha = 0$ . The higher the stream function, the faster the fluid in the cavity. Due to the high latitude of the triangular blades, the fluid inside the cavity is divided into three parts and separate vortices are formed in these parts.

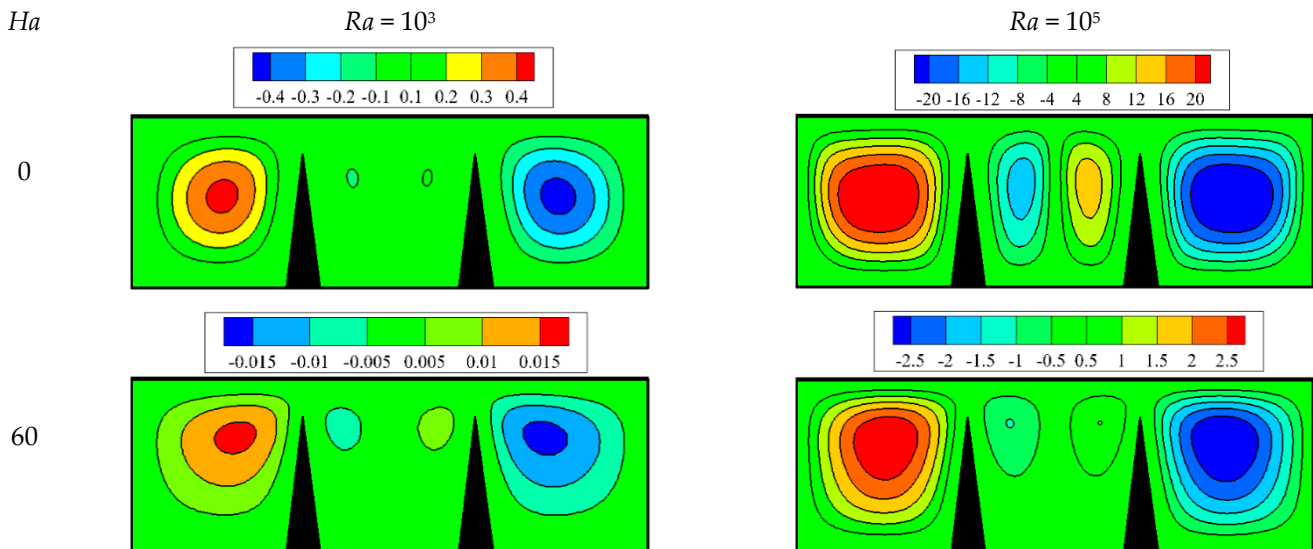


Figure 5. Velocity contours for different  $Ra$  and  $Ha$ ,  $W = 0.8$ ,  $H = 0.2$ , and 3% biological  $N/Ps$ .

Figure 6 illustrates the temperature contours for different  $Ra$  and  $Ha$ ,  $W = 0.8$ ,  $H = 0.2$ , and 3% biological  $N/Ps$ . The fluid has a low temperature at the bottom of the cavity and around the triangular blades and has a high temperature next to the upper wall. In cases where the fluid velocity in the cavity is high, the isothermal lines have more density. However, in the cavity with the low stream function, the isothermal lines are arranged uniformly as layers from top to bottom. The most regular streamlines can be seen at  $Ra = 10^3$  and  $Ha = 60$ .

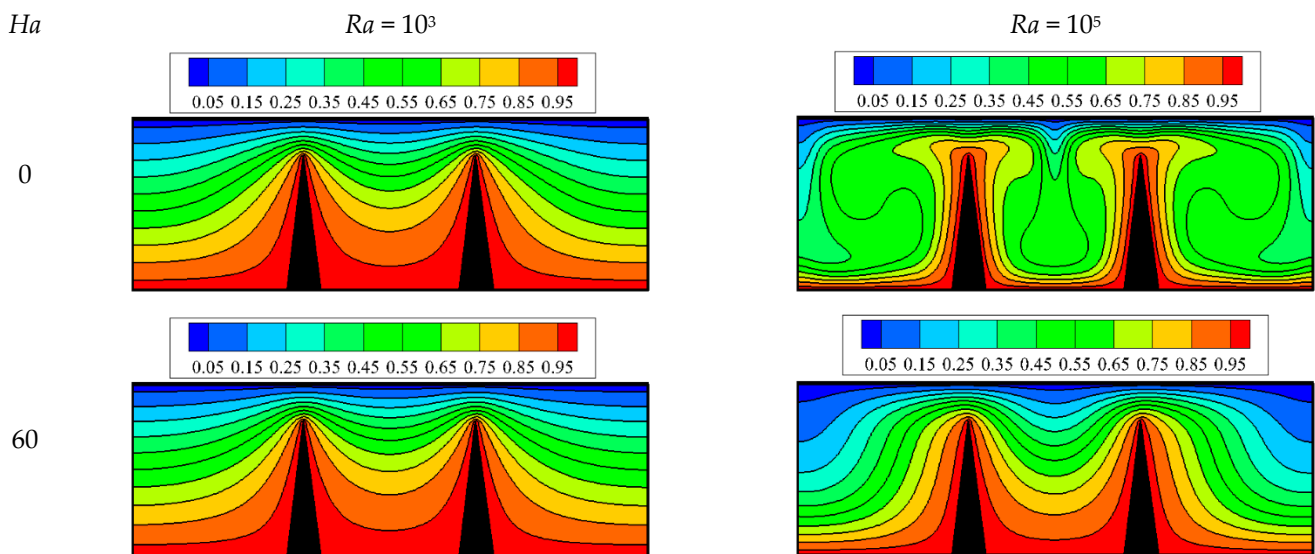


Figure 6. Temperature contours for different Rayleigh numbers and  $Ha$ s,  $W = 0.8$ ,  $H = 0.2$ , and 3% biological  $N/P$ s.

Figure 7 demonstrates the velocity contours (left) and temperature contours (right) for  $Ra = 10^5$  and  $Ha = 0$  when  $W = 0.2, 0.5$ , and  $0.8$ ,  $H = 0.2$ , and  $\varphi = 3\%$ . It can be seen that the increment in the height of the triangular blades limits the pressure for the fluid to flow in the cavity, reducing the value of the stream function. By enhancing the height of the triangular blades, the vortices in the cavity are separated and their connection with each other is reduced. When  $W = 0.8$ , a high streamline density is observed between the blade and the upper wall. At  $W = 0.2$ , the fluid rises from the right blade and descends from the top of the left blade, but at the other two heights, the fluid moves towards the upper wall from the top of both blades.

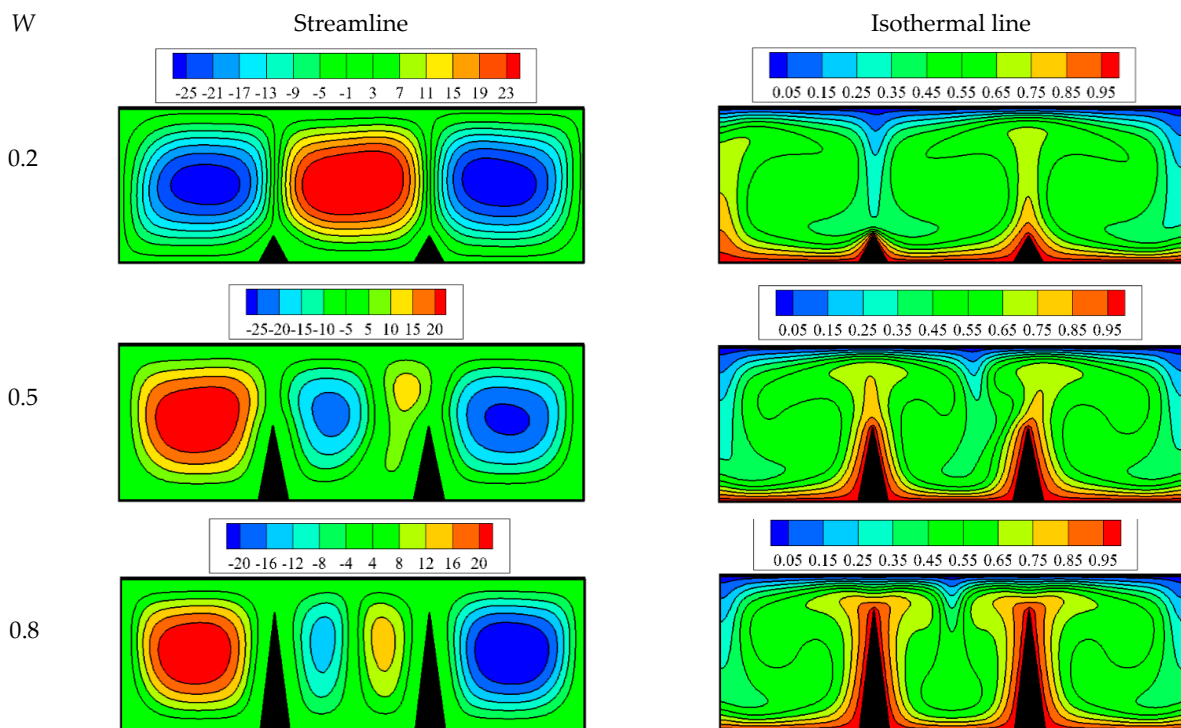
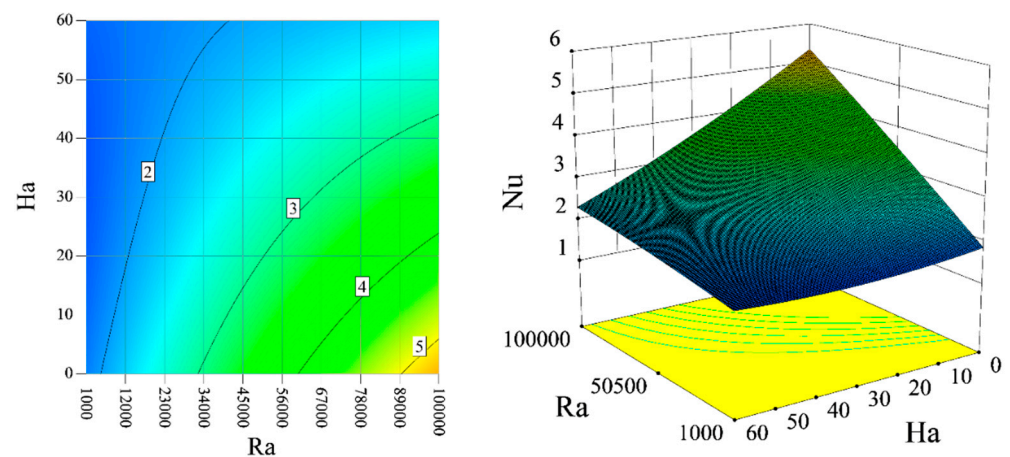


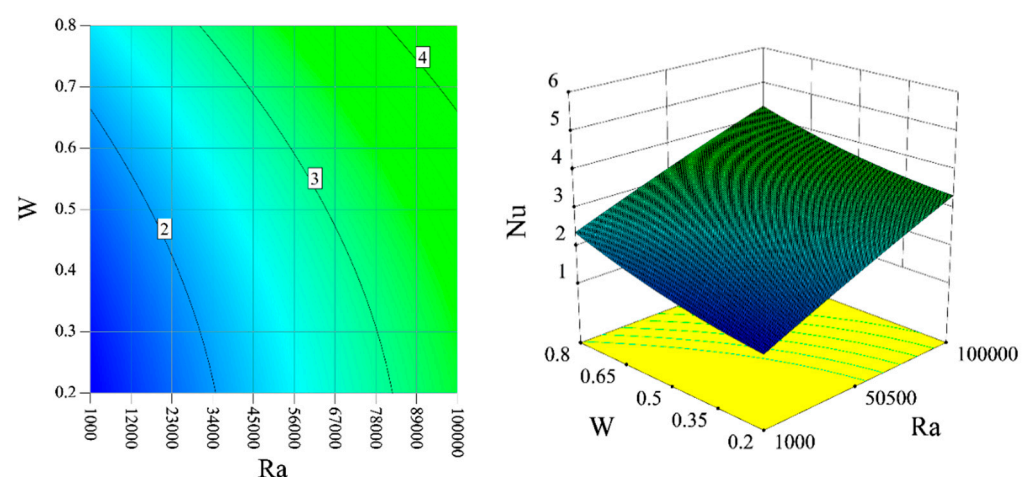
Figure 7. Velocity contours (left) and temperature contours (right) for  $Ra = 10^5$  and  $Ha = 0$  when  $W = 0.2, 0.5$ , and  $0.8$ ,  $H = 0.2$ , and  $\varphi = 3\%$ .

Figure 8 shows the  $Nu$  for different  $Ras$  and  $Has$  when  $W = 0.5$  and  $H = 0.7$  in two-dimensional (left) and three-dimensional (right) diagrams and  $\varphi = 3\%$ . An increment in the  $Ra$  from  $10^3$  to  $10^5$  enhances the value of the  $Nu$  about 2.5 times when  $Ha = 0$ . Instead, an enhancement in the  $Ha$  reduces the amount of the  $Nu$ , so that at  $Ra = 10^5$ , the decrease in the  $Nu$  is high, and at  $Ra = 10^3$ , the reduction in the  $Nu$  is low. Therefore, the maximum  $Nu$  corresponds to  $Ra = 10^5$  and  $Ha = 0$ , while the minimum one is related to  $Ra = 10^3$  and  $Ha = 60$ .



**Figure 8.**  $Nu$  for different Rayleigh numbers and  $Has$  when  $W = 0.5$  and  $H = 0.7$  in two-dimensional (left) and three-dimensional (right) diagrams and  $\varphi = 3\%$ .

Figure 9 reveals the  $Nu$  for different  $Ras$  and various blade heights when  $Ha = 30$  and  $H = 0.7$  in two-dimensional (left) and three-dimensional (right) diagrams and  $\varphi = 3\%$ . An increment in the  $Ra$  improves the  $Nu$  for all blade heights. Increasing the height of the triangular blade increases the value of the  $Nu$ . An enhancement in the height of the triangular blade causes the tip of the triangular blade to approach the cold wall from one side and increase the conduction  $H/T$ . On the other hand, there are more hot surfaces in the cavity so that the fluid collides with them and is heated. Hence, the maximum  $H/T$  occurs at  $Ra = 10^5$  and  $W = 0.8$ .

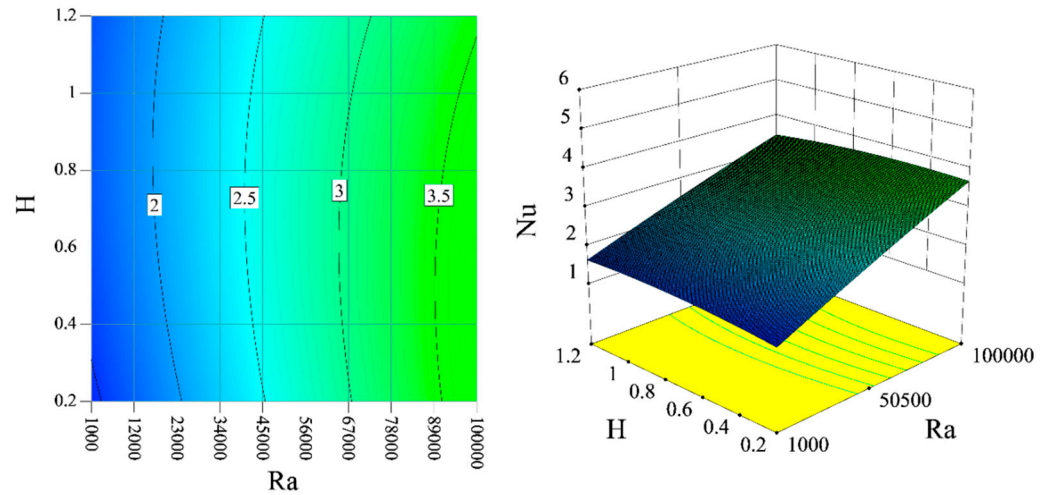


**Figure 9.**  $Nu$  for different  $Ras$  and various blade heights when  $Ha = 30$  and  $H = 0.7$  in two-dimensional (left) and three-dimensional (right) diagrams and  $\varphi = 3\%$ .

Figure 10 shows the  $Nu$  for different  $Ras$  and various values of  $H$  for  $Ha = 30$  and  $W = 0.7$  in two-dimensional (left) and three-dimensional (right) diagrams and  $\varphi = 3\%$ . It can be seen that the  $Nu$  is enhanced with the  $Ra$  for various values of  $H$ . Changes in the base of the blade lead to different trends for various  $Ras$ . The general trend of the  $Nu$

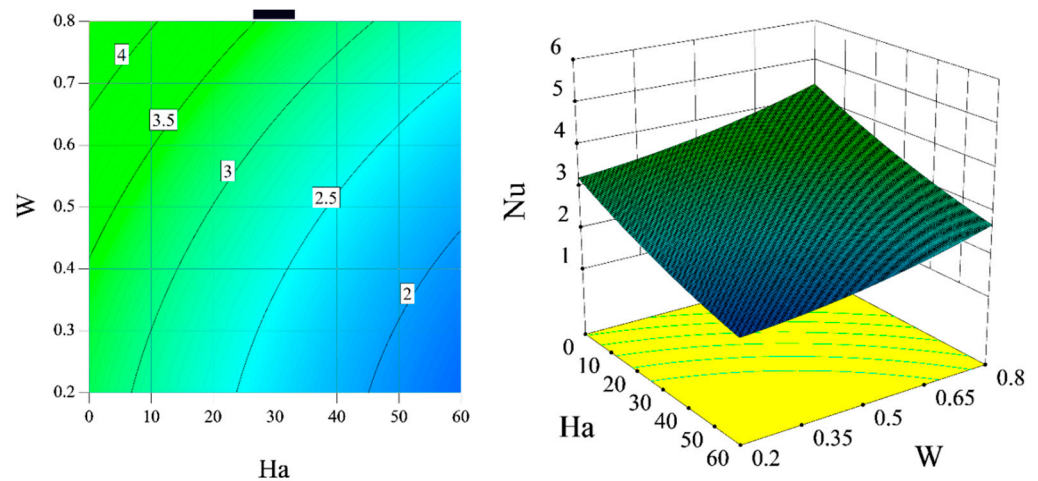


is such that it first enhances and then reduces by enhancing the base of the blade. The enhancement of the blade base to 0.7 results in an increment in the amount of  $Nu$ . At high  $Ra$ s, the Nusselt number decreases with the blade base.



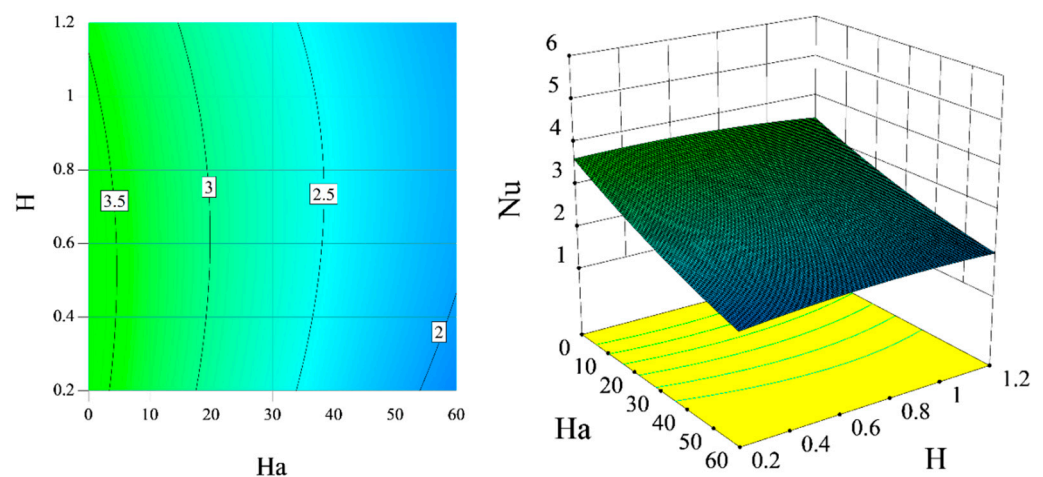
**Figure 10.**  $Nu$  for different  $Ra$ s and various values of  $H$  for  $Ha = 30$  and  $W = 0.7$  in two-dimensional (left) and three-dimensional (right) diagrams and  $\varphi = 3\%$ .

Figure 11 illustrates the  $Nu$  for different  $Ha$ s, various blade heights,  $Ra = 50,500$  and  $H = 0.7$  in two-dimensional (left) and three-dimensional (right) diagrams when  $\varphi = 3\%$ . An increment in the  $Ha$  leads to a reduction in the  $Nu$  for all blade heights. It can be seen that the  $Nu$  has an increasing trend with the blade height so that the maximum  $Nu$  corresponds to  $Ha = 0$  and  $W = 0.8$ .



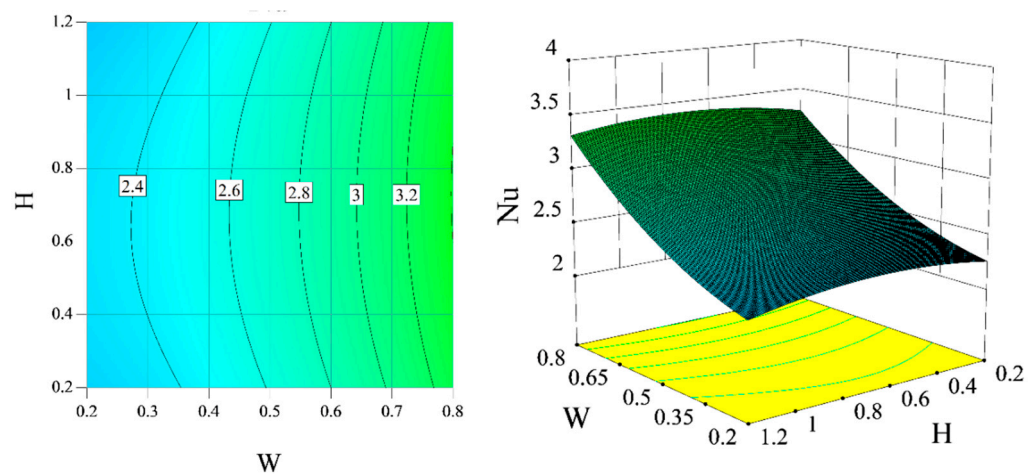
**Figure 11.**  $Nu$  for different  $Ha$ s, various blade heights,  $Ra = 50,500$  and  $H = 0.7$  in two-dimensional (left) and three-dimensional (right) diagrams when  $\varphi = 3\%$ .

Figure 12 demonstrates the  $Nu$  for different  $Ha$ s and different values of  $H$  when  $Ra = 50,500$  and  $W = 0.5$  in two-dimensional (left) and three-dimensional (right) diagrams when  $\varphi = 3\%$ . It can be seen that the  $Nu$  is reduced with the  $Ha$  for all blade bases. The variations of the  $Nu$  with the blade base are increasing and then decreasing. This trend is weak at low  $Ha$ s and the change of the  $Nu$  is low by varying the blade base, while the  $Nu$  changes considerably at high  $Ha$ s. Maximum value of  $Nu$  corresponds to  $Ha = 0$  and  $H = 0.6$ .



**Figure 12.**  $Nu$  for different  $Ha$ s and different values of  $H$  when  $Ra = 50,500$  and  $W = 0.5$  in two-dimensional (left) and three-dimensional (right) diagrams when  $\varphi = 3\%$ .

Figure 13 shows the  $Nu$  for different values of  $W$  and  $H$  when  $Ra = 50,500$  and  $Ha = 30$  in two-dimensional (left) and three-dimensional (right) diagrams when  $\varphi = 3\%$ . It can be seen that an increment in the blade height enhances the  $Nu$ , while the blade base has a different trend on the  $Nu$ . The enhancing and reducing trend of the  $Nu$  is observed by an increment in the base of the blade. The variation rate of the  $Nu$  is smaller at lower heights.



**Figure 13.**  $Nu$  for different values of  $W$  and  $H$  when  $Ra = 50,500$  and  $Ha = 30$  in two-dimensional (left) and three-dimensional (right) diagrams when  $\varphi = 3\%$ .

Table 3 presents the  $Nu$  and its changes for different volume percentages of biological  $N/Ps$  when  $Ra = 10^5$ ,  $Ha = 0$ , and  $W = H = 0.2$ . As the silver biological  $N/Ps$  are added to the water-EG mixture, the  $Nu$  is enhanced from 4.52 to 5.14. In other words, by adding 5% silver  $N/Ps$ , the  $Nu$  can be enhanced by 13.7%. The addition of biological  $N/Ps$  to water and EG mixture enhances the THCO, resulting in an enhancement in the  $Nu$ .

**Table 3.**  $Nu$  and its changes for different volume percentages of biological  $N/Ps$  when  $Ra = 10^5$ ,  $Ha = 0$ , and  $W = H = 0.2$ .

$\varphi\%$	0	1	2	3	4	5
$Nu$	4.52	4.73	4.88	4.99	5.08	5.14
$\frac{Nu_{\varphi} - Nu_{\varphi=0}}{Nu_{\varphi=0}}$	0	4.6	7.9	10.3	12.3	13.7

Eventually, a correlation is presented for the  $Nu$  in terms of the blade height and base values, as well as the Rayleigh and  $Ha$ s numbers. In this correlation, the value of the  $Nu$  can be obtained by changing each of these parameters. The parameters affecting the Nusselt number, including the Rayleigh number, Hartmann number, the height of obstacles, and the base of triangles were determined after analyzing the results. Then, these parameters were exported to one of the software for estimating the correlations, and points were provided to the user to perform recalculations. After performing 101 runs with FORTRAN software, the data were presented in the form of three-dimensional diagrams and correlations for the Nusselt number. This correlation was the best one with a minimum error than other correlations, which is discussed below:

$$\begin{aligned}
 Nu = 1.04787 & + 4.13 \times 10^{-5} Ra - 0.01 Ha + 0.154 W + 0.564 H - 4.92 \times 10^{-7} \times Ra \times Ha \\
 & - 2.14 \times 10^{-6} \times Ra \times W - 4.16 \times 10^{-6} \times Ra \times H - 5.62 \times 10^{-3} \times W \times Ha \\
 & + 5.37 \times 10^{-3} \times H \times Ha + 0.14 \times W \times H - 1.95 \times 10^{-11} \times Ra^2 \\
 & + 1.57 \times 10^{-4} \times Ha^2 + 1.8 \times W^2 - 1.8 \times H^2
 \end{aligned} \tag{18}$$

#### 4. Conclusions

In this paper, a biological  $N/Fs$  flow in a rectangular cavity with two triangular blades was simulated when a  $M/F$  was applied in the x-direction. By changing the  $Ra$  and  $Ha$ , the height, and the base values of the triangular blade, the value of the  $Nu$  was calculated. Finally, a correlation was presented for the  $Nu$ . The following are the most important findings:

1. An enhancement in the Rayleigh number from  $10^3$  to  $10^5$  intensifies the value of the Nusselt number more than 2.5 times in the absence of a magnetic field. Enhancing the Rayleigh number at all heights and bases of the triangular fin enhances the value of the Nusselt number.
2. The amount of Nusselt number decreases drastically as the magnetic field becomes stronger. This decrease is seen at high Rayleigh numbers. Increasing the Hartmann number reduces the value of the Nusselt number for different dimensions of the fin.
3. An increment in the height of the triangular fin increases the value of the Nusselt number at all Rayleigh and Hartmann numbers. This is valid at all lengths of the base of the triangular fin.
4. An increase in the base of the triangular fin first enhances (up to 0.6) and then reduces the amount of Nusselt number. This occurs at all fin heights but is more pronounced at shorter ones.
5. The addition of 5% of biological silver nanoparticles to the fluid enhances the amount of Nusselt number by 13.7% in the absence of magnetic field when  $Ra = 10^5$ .

According to this study and observing the effect of changes in the dimensions of the triangular fin on heat transfer, the effect of other shapes of fins with various dimensions can be evaluated by researchers in other articles.

**Author Contributions:** Writing—original draft and Methodology, Y.K., A.A. (Ahmad Alahmadi), A.A. (Ali Alzaed), H.A.S.; Supervision, Writing—review & editing, M.S. and G.C. All authors have read and agreed to the published version of the manuscript.

**Funding:** This work was supported by the Taif University Researchers Supporting Project, Taif University, Taif, Saudi Arabia, under Project TURSP-2020/240.

**Institutional Review Board Statement:** Not applicable.

**Informed Consent Statement:** Not applicable.

**Data Availability Statement:** Not applicable.

**Conflicts of Interest:** The authors declare no conflict of interest.

## Nomenclature

$B_0$	Magnetic field strength	
$C_p$	Specific heat [ $\text{J}/(\text{kg}\cdot\text{K})$ ]	
$g$	Gravitational acceleration [ $\text{m}/\text{s}^2$ ]	
$h$	Convection heat transfer coefficient [ $\text{W}/(\text{m}^2\cdot\text{K})$ ]	Greek symbols
$H$	Fin non-dimensional length [-]	$\alpha$ Thermal diffusivity [ $\text{m}^2/\text{s}$ ]
$Ha$	Hartmann number [-]	$\varphi$ Solid volume fraction
$k$	Thermal conductivity (THCO) [ $\text{W}/(\text{m}\cdot\text{K})$ ]	$\theta$ Temperature
$l$	Enclosure Haight [m]	$\mu$ Dynamic viscosity [ $\text{W}/(\text{m}\cdot\text{K})$ ]
$L$	Non-dimensional enclosure height [-]	$\rho$ Density [ $\text{Kg}/\text{m}^3$ ]
$l_1$	Haight of fin [m]	
$l_2$	Fin length [m]	$\sigma$ Stefan–Boltzmann constant
$Nu$	Nusselt number [-]	
$p$	Pressure [Pa]	
$P$	Non-dimensional pressure ( $\overline{P}l^2/\rho_{nf}\alpha_f^2$ )	
$Pr$	Prandtl number ( $\vartheta_f/\alpha_f$ )	
$Ra$	Rayleigh number ( $g\beta_f l^3(T_h - T_c)/\alpha_f\vartheta_f$ )	
$T$	Temperature [K]	
$u, v$	Velocity components in x and y directions [ $\text{m}/\text{s}$ ]	Subscripts
$U, V$	Velocity component ( $U = ul/\alpha_f$ , $V = vl/\alpha_f$ )	$f$ Pure fluid
$W$	Fin non-dimensional height [-]	$nf$ Nanofluid
$x, y$	Cartesian coordinates, [m]	$w$ Wall
$X, Y$	Coordinates ( $X = x/l$ , $Y = y/l$ ), [-]	

## References

- Rahimi, A.; Sepehr, M.; Lariche, M.J.; Mesbah, M.; Kasaeipoor, A.; Malekshah, E.H. Analysis of natural convection in nanofluid-filled H-shaped cavity by entropy generation and heatline visualization using lattice Boltzmann method. *Phys. E Low-Dimens. Syst. Nanostruct.* **2018**, *97*, 347–362. [\[CrossRef\]](#)
- Rahimi, A.; Kasaeipoor, A.; Malekshah, E.H.; Amiri, A. Natural convection analysis employing entropy generation and heatline visualization in a hollow L-shaped cavity filled with nanofluid using lattice Boltzmann method- experimental thermo-physical properties. *Phys. E Low-Dimens. Syst. Nanostruct.* **2018**, *97*, 82–97. [\[CrossRef\]](#)
- Aghakhani, S.; Pordanjani, A.H.; Karimipour, A.; Abdollahi, A.; Afrand, M. Numerical investigation of heat transfer in a power-law non-Newtonian fluid in a C-Shaped cavity with magnetic field effect using finite difference lattice Boltzmann method. *Comput. Fluids* **2018**, *176*, 51–67. [\[CrossRef\]](#)
- Sheremet, M.; Pop, I.; Mahian, O. Natural convection in an inclined cavity with time-periodic temperature boundary conditions using nanofluids: Application in solar collectors. *Int. J. Heat Mass Transf.* **2018**, *116*, 751–761. [\[CrossRef\]](#)
- Saeid, N.H. Natural Convection in a Square Cavity with Discrete Heating at the Bottom with Different Fin Shapes. *Heat Transf. Eng.* **2018**, *39*, 154–161. [\[CrossRef\]](#)
- Revnin, C.; Abu-Nada, E.; Grosan, T.; Pop, I. Natural convection in a rectangular cavity filled with nanofluids: Effect of variable viscosity. *Int. J. Numer. Methods Heat Fluid Flow* **2018**, *28*, 1410–1432. [\[CrossRef\]](#)
- Nezhad, S.M.; Rezaniakolaei, A.; Shadloo, M.S.; Rosendahl, L.A. Adiabatic partition effect on natural convection heat transfer inside a square cavity: Experimental and numerical studies. *Heat Mass Transf./Wärme-Und Stoffuebertragung* **2018**, *54*, 291–304.
- Das, D.; Lukose, L.; Basak, T. Role of multiple solar heaters along the walls for the thermal management during natural convection in square and triangular cavities. *Renew. Energy* **2018**, *121*, 205–229. [\[CrossRef\]](#)
- Parsa, S.M.; Rahbar, A.; Javadi, D.Y.; Koleini, M.H.; Afrand, M.; Amidpour, M. Energy-matrices, exergy, economic, environmental, exergoeconomic, enviroeconomic, and heat transfer (6E/HT) analysis of two passive/active solar still water desalination nearly 4000m: Altitude concept. *J. Clean. Prod.* **2020**, *261*, 121243. [\[CrossRef\]](#)
- Parsa, S.M.; Rahbar, A.; Koleini, M.; Aberoumand, S.; Afrand, M.; Amidpour, M. A renewable energy-driven thermoelectric-utilized solar still with external condenser loaded by silver/nanofluid for simultaneously water disinfection and de-salination. *Desalination* **2020**, *480*, 114354. [\[CrossRef\]](#)
- Parsa, S.M.; Rahbar, A.; Koleini, M.; Javadi, Y.D.; Afrand, M.; Rostami, S.; Amidpour, M. First approach on nanofluid-based solar still in high altitude for water desalination and solar water disinfection (SODIS). *Desalination* **2020**, *491*, 114592. [\[CrossRef\]](#)
- Pordanjani, A.H.; Aghakhani, S.; Afrand, M.; Sharifpur, M.; Meyer, J.P.; Xu, H.; Ali, H.M.; Karimi, N.; Cheraghian, G. Nanofluids: Physical phenomena, applications in thermal systems and the environment effects—A critical review. *J. Clean. Prod.* **2021**, *320*, 128573. [\[CrossRef\]](#)
- Mahdavi, M.; Garbadeen, I.; Sharifpur, M.; Ahmadi, M.H.; Meyer, J.P. Study of particle migration and deposition in mixed convective pipe flow of nanofluids at different inclination angles. *J. Therm. Anal. Calorim.* **2019**, *135*, 1563–1575. [\[CrossRef\]](#)

14. Rostami, S.; Kalbasi, R.; Talebkeikhah, M.; Goldanlou, A.S. Improving the thermal conductivity of ethylene glycol by addition of hybrid nano-materials containing multi-walled carbon nanotubes and titanium dioxide: Applicable for cooling and heating. *J. Therm. Anal. Calorim.* **2021**, *143*, 1701–1712. [[CrossRef](#)]
15. Afrand, M. Using a magnetic field to reduce natural convection in a vertical cylindrical annulus. *Int. J. Therm. Sci.* **2017**, *118*, 12–23. [[CrossRef](#)]
16. Afrand, M.; Farahat, S.; Nezhad, A.H.; Sheikhzadeh, G.A.; Sarhaddi, F. 3-D numerical investigation of natural convection in a tilted cylindrical annulus containing molten potassium and controlling it using various magnetic fields. *Int. J. Appl. Mech.* **2014**, *46*, 809–821.
17. Afrand, M.; Farahat, S.; Nezhad, A.H.; Sheikhzadeh, G.A.; Sarhaddi, F.; Wongwises, S. Multi-objective optimization of natural convection in a cylindrical annulus mold under magnetic field using particle swarm algorithm. *Int. Commun. Heat Mass Transf.* **2015**, *60*, 13–20. [[CrossRef](#)]
18. Giwa, S.O.; Sharifpur, M.; Ahmadi, M.H.; Meyer, J.P. A review of magnetic field influence on natural convection heat transfer performance of nanofluids in square cavities. *J. Therm. Anal. Calorim.* **2021**, *145*, 2581–2623. [[CrossRef](#)]
19. Ampofo, F. Turbulent natural convection in an air filled partitioned square cavity. *Int. J. Heat Fluid Flow* **2004**, *25*, 103–114. [[CrossRef](#)]
20. Selimefendigil, F.; Öztop, H.F. Corrugated conductive partition effects on MHD free convection of CNT-water nanofluid in a cavity. *Int. J. Heat Mass Transf.* **2019**, *129*, 265–277. [[CrossRef](#)]
21. Selimefendigil, F.; Öztop, H.F. MHD Natural Convection and Entropy Generation in a Nanofluid-Filled Cavity with a Conductive Partition. In *Exergetic, Energetic and Environmental Dimensions*; Elsevier BV: Amsterdam, The Netherlands, 2018; pp. 763–778.
22. Selimefendigil, F.; Öztop, H.F. Natural convection and entropy generation of nanofluid filled cavity having different shaped obstacles under the influence of magnetic field and internal heat generation. *J. Taiwan Inst. Chem. Eng.* **2015**, *56*, 42–56. [[CrossRef](#)]
23. Selimefendigil, F.; Öztop, H.F.; Chamkha, A.J. MHD mixed convection in a nanofluid filled vertical lid-driven cavity having a flexible fin attached to its upper wall. *J. Therm. Anal. Calorim.* **2019**, *135*, 325–340. [[CrossRef](#)]
24. Dogonchi, A.S.; Chamkha, A.J.; Ganji, D.D. A numerical investigation of magneto-hydrodynamic natural convection of Cu–water nanofluid in a wavy cavity using CVFEM. *J. Therm. Anal. Calorim.* **2019**, *135*, 2599–2611. [[CrossRef](#)]
25. Dogonchi, A.S.; Ismael, M.A.; Chamkha, A.J.; Ganji, D.D. Numerical analysis of natural convection of Cu–water nanofluid filling triangular cavity with semicircular bottom wall. *J. Therm. Anal. Calorim.* **2019**, *135*, 3485–3497. [[CrossRef](#)]
26. Pordanjani, A.H.; Aghakhani, S. Numerical Investigation of Natural Convection and Irreversibilities between Two Inclined Concentric Cylinders in Presence of Uniform Magnetic Field and Radiation. *Heat Transf. Eng.* **2021**, *1*, 1–21. [[CrossRef](#)]
27. Pordanjani, A.H.; Aghakhani, S.; Afrand, M.; Mahmoudi, B.; Mahian, O.; Wongwises, S. An updated review on application of nanofluids in heat exchangers for saving energy. *Energy Convers. Manag.* **2019**, *198*, 111886. [[CrossRef](#)]
28. Mahdavi, M.; Sharifpur, M.; Ghodsinezhad, H.; Meyer, J.P. Experimental and Numerical Investigation on a Water-Filled Cavity Natural Convection to Find the Proper Thermal Boundary Conditions for Simulations. *Heat Transf. Eng.* **2018**, *39*, 359–373. [[CrossRef](#)]
29. Sharifpur, M.; Solomon, A.B.; Ottermann, T.L.; Meyer, J.P. Optimum concentration of nanofluids for heat transfer enhancement under cavity flow natural convection with TiO<sub>2</sub>—Water. *Int. Commun. Heat Mass Transf.* **2018**, *98*, 297–303. [[CrossRef](#)]
30. Aybar, H.Ş.; Sharifpur, M.; Azizian, M.R.; Mehrabi, M.; Meyer, J.P. A Review of Thermal Conductivity Models for Nanofluids. *Heat Transf. Eng.* **2015**, *36*, 1085–1110. [[CrossRef](#)]
31. Shi, C.; Zhang, X.; Zhang, X.; Chen, P.; Xu, L. Ultrasonic desulfurization of amphiphilic magnetic-Janus nanosheets in oil-water mixture system. *Ultrason. Sonochem.* **2021**, *76*, 105662. [[CrossRef](#)]
32. Tian, M.-W.; Rostami, S.; Aghakhani, S.; Goldanlou, A.S.; Qi, C. A techno-economic investigation of 2D and 3D configurations of fins and their effects on heat sink efficiency of MHD hybrid nanofluid with slip and non-slip flow. *Int. J. Mech. Sci.* **2021**, *189*, 105975. [[CrossRef](#)]
33. Yan, S.-R.; Aghakhani, S.; Karimipour, A. Influence of a membrane on nanofluid heat transfer and irreversibilities inside a cavity with two constant-temperature semicircular sources on the lower wall: Applicable to solar collectors. *Phys. Scr.* **2020**, *95*, 085702. [[CrossRef](#)]
34. Vafaei, M.; Afrand, M.; Sina, N.; Kalbasi, R.; Sourani, F.; Teimouri, H. Evaluation of thermal conductivity of MgO-MWCNTs/EG hybrid nanofluids based on experimental data by selecting optimal artificial neural networks. *Phys. E Low-Dimens. Syst. Nanostruct.* **2017**, *85*, 90–96. [[CrossRef](#)]
35. Shahrestani, M.I.; Maleki, A.; Shadloo, M.S.; Tlili, I. Numerical Investigation of Forced Convective Heat Transfer and Performance Evaluation Criterion of Al<sub>2</sub>O<sub>3</sub>/Water Nanofluid Flow inside an Axisymmetric Microchannel. *Symmetry* **2020**, *12*, 120. [[CrossRef](#)]
36. Ghalandari, M.; Maleki, A.; Haghighi, A.; Shadloo, M.S.; Nazari, M.A.; Tlili, I. Applications of nanofluids containing carbon nanotubes in solar energy systems: A review. *J. Mol. Liq.* **2020**, *313*, 113476. [[CrossRef](#)]
37. Cheraghian, G. Improved heavy oil recovery by nanofluid surfactant flooding—An experimental study. *Eur. Assoc. Geosci. Eng.* **2016**, *2016*, 1–5. [[CrossRef](#)]
38. Wang, N.; Maleki, A.; Nazari, M.A.; Tlili, I.; Shadloo, M.S. Thermal Conductivity Modeling of Nanofluids Contain MgO Particles by Employing Different Approaches. *Symmetry* **2020**, *12*, 206. [[CrossRef](#)]
39. Nezhad, S.S.K.; Bazgir, S. Improvement of thermal stability of polyacryl amide solution used as a nano-fluid in enhanced oil recovery process by nanoclay. *Int. J. Nanosci. Nanotechnol.* **2015**, *11*, 201–208.

40. Bahiraei, M.; Heshmatian, S.; Keshavarzi, M. A decision-making based method to optimize energy efficiency of ecofriendly nanofluid flow inside a new heat sink enhanced with flow distributor. *Powder Technol.* **2019**, *342*, 85–98. [[CrossRef](#)]
41. Yang, L.; Huang, J.-N.; Mao, M.; Ji, W. Numerical assessment of Ag-water nano-fluid flow in two new microchannel heatsinks: Thermal performance and thermodynamic considerations. *Int. Commun. Heat Mass Transf.* **2020**, *110*, 104415. [[CrossRef](#)]
42. Bahiraei, M.; Heshmatian, S. Thermal performance and second law characteristics of two new microchannel heat sinks operated with hybrid nanofluid containing graphene–silver nanoparticles. *Energy Convers. Manag.* **2018**, *168*, 357–370. [[CrossRef](#)]
43. Mashayekhi, R.; Khodabandeh, E.; Bahiraei, M.; Bahrami, L.; Toghraie, D.; Akbari, O.A. Application of a novel conical strip insert to improve the efficacy of water–Ag nanofluid for utilization in thermal systems: A two-phase simulation. *Energy Convers. Manag.* **2017**, *151*, 573–586. [[CrossRef](#)]
44. Bahiraei, M.; Heshmatian, S. Application of a novel biological nanofluid in a liquid block heat sink for cooling of an electronic processor: Thermal performance and irreversibility considerations. *Energy Convers. Manag.* **2017**, *149*, 155–167. [[CrossRef](#)]
45. Sheikholeslami, M.; Hayat, T.; Muhammad, T.; Alsaedi, A. RETRACTED: MHD forced convection flow of nanofluid in a porous cavity with hot elliptic obstacle by means of Lattice Boltzmann method. *Int. J. Mech. Sci.* **2018**, *135*, 532–540. [[CrossRef](#)]
46. Kefayati, G.; Tang, H. MHD thermosolutal natural convection and entropy generation of Carreau fluid in a heated enclosure with two inner circular cold cylinders, using LBM. *Int. J. Heat Mass Transf.* **2018**, *126*, 508–530. [[CrossRef](#)]
47. Li, X.; Dong, Z.-Q.; Yu, P.; Wang, L.-P.; Niu, X.-D.; Yamaguchi, H.; Li, D.-C. Effect of self-assembly on fluorescence in magnetic multiphase flows and its application on the novel detection for COVID-19. *Phys. Fluids* **2021**, *33*, 042004. [[CrossRef](#)] [[PubMed](#)]
48. Aghakhani, S.; Ghasemi, B.; Pordanjani, A.H.; Wongwises, S.; Afrand, M. Effect of replacing nanofluid instead of water on heat transfer in a channel with extended surfaces under a magnetic field. *Int. J. Numer. Methods Heat Fluid Flow* **2019**, *29*, 1249–1271. [[CrossRef](#)]
49. Aminossadati, S. Hydromagnetic natural cooling of a triangular heat source in a triangular cavity with water–CuO nanofluid. *Int. Commun. Heat Mass Transf.* **2013**, *43*, 22–29. [[CrossRef](#)]
50. Sheikholeslami, M.; Hayat, T.; Alsaedi, A. Numerical simulation for forced convection flow of MHD CuO–H<sub>2</sub>O nanofluid inside a cavity by means of LBM. *J. Mol. Liq.* **2018**, *249*, 941–948. [[CrossRef](#)]
51. Sivaraj, C.; Sheremet, M. MHD natural convection and entropy generation of ferrofluids in a cavity with a non-uniformly heated horizontal plate. *Int. J. Mech. Sci.* **2018**, *149*, 326–337. [[CrossRef](#)]
52. Chamkha, A.J.; Aly, A.M. MHD Free Convection Flow of a Nanofluid Past a Vertical Plate in the Presence of Heat Generation or Absorption Effects. *Chem. Eng. Commun.* **2010**, *198*, 425–441. [[CrossRef](#)]
53. Pordanjani, A.H.; Jahanbakhshi, A.; Nadooshan, A.A.; Afrand, M. Effect of two isothermal obstacles on the natural convection of nanofluid in the presence of magnetic field inside an enclosure with sinusoidal wall temperature distribution. *Int. J. Heat Mass. Transf.* **2018**, *121*, 565–578. [[CrossRef](#)]
54. Sheikholeslami, M.; Ganji, D.D. Entropy generation of nanofluid in presence of magnetic field using Lattice Boltzmann Method. *Phys. A Stat. Mech. Appl.* **2015**, *417*, 273–286. [[CrossRef](#)]
55. Pak, B.C.; Cho, Y.I. Hydrodynamic and Heat Transfer Study of Dispersed Fluids with Submicron Metallic Oxide Particles. *Exp. Heat Transf.* **1998**, *11*, 151–170. [[CrossRef](#)]
56. Bhanvase, B.A.; Sarode, M.R.; Putterwar, L.A.; Abdullah, K.A.; Deosarkar, M.P.; Sonawane, S.H. Sonawane. Intensification of convective heat transfer in water/ethylene glycol based nanofluids containing TiO<sub>2</sub> nanoparticles. *Chem. Eng. Process. Process Intensif.* **2014**, *82*, 123–131. [[CrossRef](#)]
57. Sarafraz, M.; Hormozi, F. Intensification of forced convection heat transfer using biological nanofluid in a double-pipe heat exchanger. *Exp. Therm. Fluid Sci.* **2015**, *66*, 279–289. [[CrossRef](#)]
58. Natsuki, J.; Natsuki, T.; Hashimoto, Y. A Review of Silver Nanoparticles: Synthesis Methods, Properties and Applications. *Int. J. Mater. Sci. Appl.* **2015**, *4*, 325. [[CrossRef](#)]
59. Natsuki, T.; Natsuki, J. One-Step Synthesis of Silver Nanoparticles Using Low Molecular Weight Compounds at Room Temperature. *Int. J. Mater. Eng. Technol.* **2015**, *13*, 109–119. [[CrossRef](#)]
60. Żyła, G.; Fal, J. Viscosity, thermal and electrical conductivity of silicon dioxide–ethylene glycol transparent nanofluids: An experimental studies. *Thermochim. Acta* **2017**, *650*, 106–113. [[CrossRef](#)]
61. Oztop, H.F.; Abu-Nada, E. Numerical study of natural convection in partially heated rectangular enclosures filled with nanofluids. *Int. J. Heat Fluid Flow* **2008**, *29*, 1326–1336. [[CrossRef](#)]